applied sciences

MDPI

Article

Compact Beam-Scanning Reflectarray Antenna with SLL Reduction Using In-Plane Panel Translations

Andrés Gómez-Álvarez [1], Sérgio A. Matos [2], Manuel Arrebola [3,*], Marcos R. Pino [1] and Carlos A. Fernandes [4]

[1] Department of Electrical Engineering, Group of Signal Theory and Communications, University of Oviedo, 33203 Gijón, Spain; andresga@uniovi.es (A.G.-Á.); mpino@uniovi.es (M.R.P.)
[2] Instituto de Telecomunicações and the Departamento de Ciências e Tecnologias da Informaçao, Instituto Universitário de Lisboa (Iscte-IUL), 1649-026 Lisbon, Portugal; sergio.matos@iscte-iul.pt
[3] Department of Signals, Systems and Radiocommunications, Group of Applied Electromagnetics, Universidad Politécnica de Madrid, 28040 Madrid, Spain
[4] Instituto de Telecomunicações, Instituto Superior Técnico, Universidade de Lisboa, 1049-001 Lisbon, Portugal; carlos.fernandes@lx.it.pt
* Correspondence: manuel.arrebola@upm.es

Abstract: A mechanical beam-scanning reflectarray (RA) antenna is presented for Ka band. The 1D steering of the beam is achieved through linear in-plane panel translations, which can be implemented at low cost using a rail-mounted moving RA panel. Compared to related works, a highly uniform beam level is achieved with a remarkably compact antenna profile. A new technique is also proposed to mitigate the high side lobes caused by the compact antenna optics, achieving an estimated 2.3 dB reduction in maximum SLL. The manufactured prototype has a panel size of 256.4 by 187.2 mm with 2898 elements, and an F/D of only 0.47. A measured scan loss of 1.1 dB is achieved over a 45-degree scanning range. The measured gain is 31.6 dBi and the aperture efficiency is 24.7% at the design frequency of 29.5 GHz, with SLL between −9.4 and −17.5 dB. In-band measurements show a 1 dB bandwidth from 28 to over 32 GHz (11.9%).

Keywords: reflectarray antennas; steerable antennas; mechanical beam steering; mm-wave

Academic Editors: Paola Pirinoli and Michele Beccaria

Received: 1 March 2025
Revised: 31 March 2025
Accepted: 9 April 2025
Published: 11 April 2025

Citation: Gómez-Álvarez, A.; Matos, S.A.; Arrebola, M.; Pino, M.R.; Fernandes, C.A. Compact Beam-Scanning Reflectarray Antenna with SLL Reduction Using In-Plane Panel Translations. *Appl. Sci.* **2025**, *15*, 4244. https://doi.org/10.3390/app15084244

1. Introduction

Modern low Earth orbit (LEO) satellite communication systems are reshaping broadband connectivity by providing global coverage with reduced latency compared to traditional geostationary (GEO) high-throughput satellites (HTSs). These systems offer greater flexibility and scalability by relying on gradually deployable and expandable constellations of smaller satellites [1]. LEO constellations require highly flexible user terminals capable of continuous beam tracking to maintain seamless connectivity with fast-moving satellites. Small phased arrays are often used to achieve this reconfigurability, as traditional parabolic reflector antennas cannot provide the wide-angle scanning required for this application [2]. However, these terminals face particularly stringent cost requirements to allow mass adoption, and thus, reducing their complexity is a major priority [3].

Spatially fed arrays (SFAs) are positioned as a competitive solution for modern reconfigurable mm-wave terminals. Low manufacturing costs are enabled by mature PCB [4–6] or 3D-printing [7–9] technologies for the array elements. Furthermore, the use of low-profile planar surfaces allows for easy stowage and integration to various platforms [10,11]. Electronically reconfigurable antennas can be achieved by introducing active components

to the array elements, e.g., via integrated electronics [12–14] or MEMS [15,16]. These however add costly components and control circuitry, sacrificing part of the simplicity and affordability of SFAs. Alternatively, multiple feeding elements can be used to illuminate a passive SFA, each one steering the beam in a different direction. Beam switching can then be used to steer the beam, at the expense of complex feeding configurations and antenna optics [17–19].

Mechanical beam steering is a more accessible option that relies on translations and rotations of the feed or panel, trading mechanical complexity and lower aperture efficiency for affordability and a simpler control system with a significantly lower power consumption. Some implementations based on Risley prisms use two co-axially rotating surfaces to achieve 2D steering at the expense of the complexity and losses of two SFAs [20–22]. One-dimensional wide-angle steering can be achieved by moving the feed along a focal arc while pointed towards a fixed point on the aperture [23–26]. Another common approach that prioritizes mechanical simplicity relies on linear panel translations to achieve 1D steering [9,27], avoiding movements and re-orientations of the feeding RF chain. This improves the long-term reliability of the system at the cost of requiring a larger antenna volume to support the movements of the panel.

This work presents a compact and cost-effective RA antenna capable of 1D beam scanning in the Ka band. In-plane panel translations are used to steer the beam. This scanning approach excels in mechanical simplicity, requiring only a light rail-mounted panel controlled by a low-power motor. An iterative process is used to design the phase response of the RA, progressively expanding its steering range while controlling its scan losses. At every iteration, the radiation requirements are updated and the phase response of the RA is adjusted using a multi-focal optimization algorithm. Once a range of 45 degrees is achieved, a novel technique is proposed to reduce the SLLs. The phase response is refined to avoid partially collimating phase patterns in the directions where the highest side lobes are predicted, achieving an estimated reduction in maximum SLL of 2.3 dB. Despite having an F/D of only 0.47, the antenna achieves a low measured scan loss of 1.1 dB and a moderate gain of 31.6 dBi at 29.5 GHz.

2. Antenna Definition

The geometry of the presented antenna is shown in Figure 1. One-dimensional steering is achieved through in-plane linear panel translations, which are used to control the portion of the aperture that is illuminated. The position of the center of the panel is defined by an offset d in the x-axis, which relates to the steering angle. The feed is a commercial 11.5 dBi linear-polarized rectangular horn, model LB-28-10-C-KF from A-INFOMW. It is selected to achieve a compact setup thanks to its low directivity. The feed is located at $x_f = -66.1$ mm, and a tilt of $\alpha = 26^\circ$ is introduced to avoid the beam distortions caused by feed blockage for the beam steering angles $\theta \geq 0^\circ$ in the XZ-plane. The feed-to-panel distance F is set to 88 mm, or 8.66 λ_0, at the design frequency of 29.5 GHz, and the size of the panel orthogonal to the translation is set to $D_y = 187.2$ mm. These two values result in an illumination taper of -11.6 dB on the longer panel sides and a very low F/D_y ratio of 0.47. The E-plane of the feed and the reflected beam coincides with the XZ-plane for all beam directions.

Designing an RA relies on the accurate modeling of the electromagnetic field on the panel. For any given panel position, the incident field is obtained from a full-wave HFSS simulation using Ansys HFSS (Release 2023R1) [28]. The tangential reflected and incident field components can then be related at each cell of the lattice as follows [29]:

$$\begin{pmatrix} E_x^r(\vec{r}_n) \\ E_y^r(\vec{r}_n) \end{pmatrix} = \begin{pmatrix} \rho_{n,xx} & \rho_{n,xy} \\ \rho_{n,yx} & \rho_{n,yy} \end{pmatrix} \cdot \begin{pmatrix} E_x^i(\vec{r}_n) \\ E_y^i(\vec{r}_n) \end{pmatrix}, \quad (1)$$

where $\vec{r}_n = (x_n, y_n, z_n)$ is the position of the n-th element. $\rho_{n,xx}$ and $\rho_{n,yy}$ are its direct linear reflection coefficients, which can typically be approximated as the ideal phase shifters, $e^{j\phi_{n,x|y}}$. Furthermore, the cross-polarization coefficients ρ_{xy} and ρ_{yx} can be neglected if a cell with good polarization purity is selected. This simplifies the design process into selecting the shifts $\phi_{n,x|y}$ that each element should introduce. For the presented antenna geometry and polarization, the focus is on the $\phi_{n,x}$ phase response, and the x-notation will be dropped for clarity. To avoid grating lobes, square cells of side $p = 0.4\lambda_0$ (4.07 mm) are considered in the following analysis.

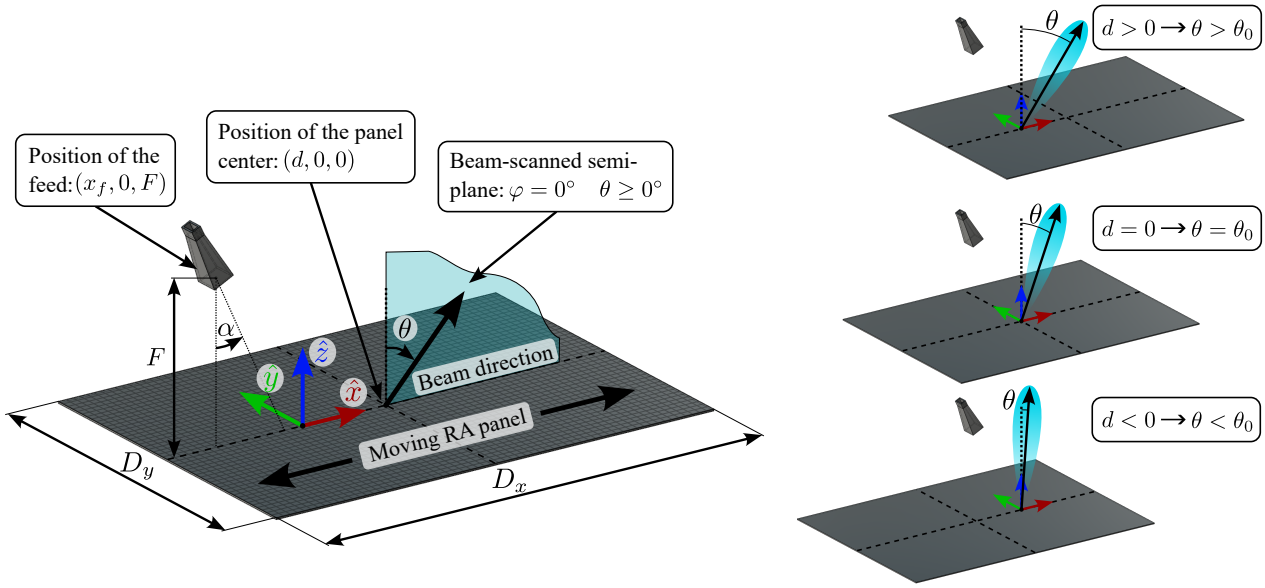

Figure 1. Mechanical beam-scanning RA antenna using linear in-plane movements: antenna optics (**left**) and illustration of the relation between the panel position and the steering angle (**right**).

It is known from array theory that beam collimation requires a progressive linear phase on the reflected field [30]. This can be achieved by selecting the phase shift for each cell to compensate for the delay of the impinging field, $\angle E^i_x(\vec{r}_n)$. When the panel is at an arbitrary position d, and particularizing for $\varphi = 0°$ for the intended scanned plane, the maximum collimation towards a direction θ_0 requires a phase law

$$\phi_n = -k_0 x_n \sin\theta_0 - \angle E^i_x(\vec{r}_n). \tag{2}$$

As the panel shifts out of this position, the beam is de-focused, changing its gain and pointing angle. To estimate the radiation performance of a given phase law and panel position, the incident field is first obtained for that panel position. Then, the reflected field on the panel is calculated using (1), assuming the phase shifting elements are ideal. Then, the radiation pattern is calculated using the second principle of equivalence, as described in [31]. To analyze the continuous translation path, it is discretized into finely spaced positions. For convenience, the discretization step is selected to match the element spacing p. The notation d_k will be used to identify the position of the panel $d_k = k \cdot p$.

3. Multi-Stage Design

In order to achieve good scanning performance, the RA response needs to be tailored to the entire panel translation path, rather than to a fixed position and radiation angle. This path can be discretized into a set of positions $\bar{d} = \{d_0, d_{\pm1}, d_{\pm2}, \ldots\}$, each with a matching radiation angle θ_k. For every (d_k, θ_k) pair, a unifocal phase law can be calculated using (2). Then, a multi-focal optimization algorithm is required to calculate a single phase law for the RA panel that achieves a balanced radiation performance among several panel positions.

The multi-focal phase law should mitigate the beam de-focusing effects as the panel is translated, equalizing the performance across the entire translation range. In doing so, a drop in maximum gain and increased beam distortion are to be expected compared to a unifocal non-scanning design, as the panel cannot be fully tailored to any one specific focal position.

In multi-focal designs, introducing a carefully selected phase reference $\Delta\phi_k$ to each unifocal phase law before the optimization process can yield significant performance improvements [19,24]. The selection of these phase references can be integrated into the optimization, but this typically requires a complex optimization algorithm to handle the simultaneous tuning of the entire phase law (i.e., the phase response of every cell), in addition to the phase references. This is a slow and complex process that can impose a limit on the number of panel positions being considered. An alternative is introduced in [17] with the multi-feed phase-only optimization algorithm (MF-POO), which will be used as part of the design process presented below. This algorithm is a multi-focal technique that integrates the phase references into the optimization process. However, it does so without requiring a large optimization process, as it relies on a series of much faster single-parameter optimizations to iteratively find the optimal solution. This reduces computational costs, while enabling the optimization of many panel positions to ensure stable antenna performance. MF-POO also introduces a weighting factor w_k to each configuration being optimized (i.e., each panel position for the presented antenna geometry). These can be adjusted to control the influence of each unifocal phase law in the optimization process, which in turn enables the fine control over the scan loss for a set of panel positions. Because of its fast convergence and the ability to control the scanning losses, MF-POO will be selected over other multi-focal optimization algorithms for the optimization process described below.

3.1. Scanning Range Enhancement

A major design challenge of the proposed antenna geometry is that it is not clear how to relate the panel positions d_k and the beam directions θ_k to achieve good scanning performance. As a result, a multi-focal optimization cannot be directly used to calculate the final phase law. Instead, the iterative process represented in Figure 2 is used, where the translation range is gradually expanded while reinforcing the natural beam scanning of the antenna geometry. The exact panel size required to accommodate the final translation range is initially unknown, so D_x is purposefully overestimated at this point.

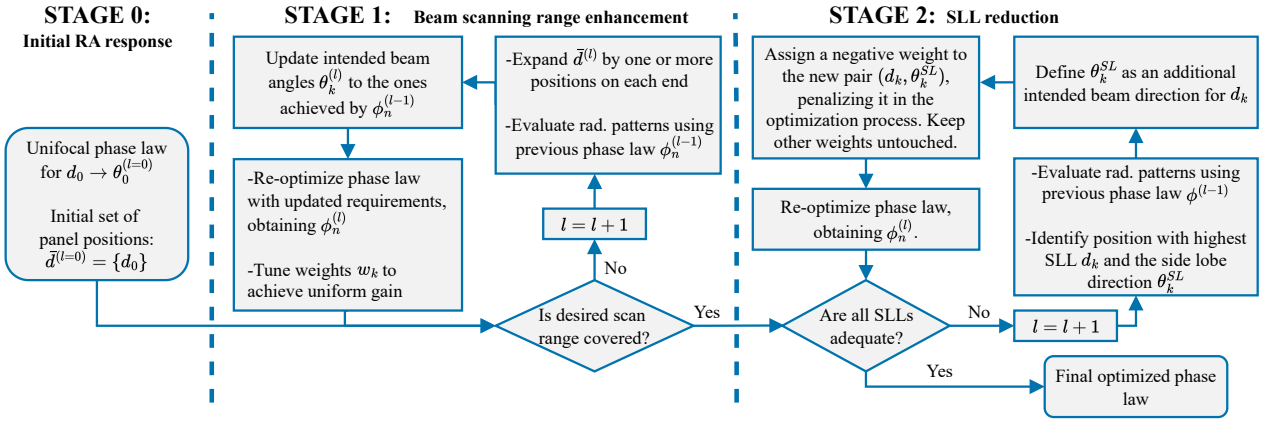

Figure 2. Multi-stage optimization process of the RA response.

The design process starts with a unifocal analytical phase law for d_0 and a beam angle of $\theta_0 = 26°$, calculated using (2). The scanning performance of this phase law is evaluated

by calculating the radiation pattern for panel positions close to d_0:$d_{\pm1}$, $d_{\pm2}$, and $d_{\pm3}$. These positions are selected as the first set of positions to optimize. For each of these positions d_k, an intended radiation direction θ_k is assigned. This intended direction matches the beam direction observed for the unifocal phase law. Having defined a set of positions and intended directions, the first multi-focal optimization can be performed to calculate a new phase law that equalizes the gain level for this small set of panel positions.

The above process is repeated until a beam steering range from 0° to 45° is covered. For every l-th iteration, the set of panel positions is expanded. Then, the radiation performance of the previous phase law, $\phi_n^{(l-1)}$, is evaluated at every panel position in the updated set. The intended beam direction θ_k for every position is the calculated beam direction from the previous phase law. This reinforces the natural tilting of the beam, and it gradually updates the relation between the panel position and the beam pointing. Once the set of panel positions and its associated set of intended radiation directions are updated, another multi-focal optimization is performed to calculate a new phase law $\phi_n^{(l)}$. In doing so, the weighting factors of every position w_k are tuned to ensure that scanning losses remain below 1.5 dB in the new optimized range.

This process is repeated for a total of nine iterations, requiring 24 panel positions from d_{-12} to d_{11}. The panel positions being considered and the intended radiation direction for each of them are listed in Table 1. Six positions are introduced in the first iteration (three on each side of d_0) and four in the second. Starting with iteration 3, only one position is introduced on each side of the previous translation range to ensure a slow and gradual increase in scanning range and to improve the convergence of the optimization algorithm. This iterative design technique progressively expands the usable beam steering range and adapts the radiation angles for each position.

Table 1. Intended radiation direction θ_k (in degrees) for each panel position throughout the optimization process. The red numbers indicate secondary radiation directions which are assigned a negative optimization weight to mitigate specific side lobes.

	Iteration l		**Stage 1**									**Stage 2**	
		0	**1**	**2**	**3**	**4**	**5**	**6**	**7**	**8**	**9**	**10**	**11**
Panel position d_k	d_{-12}	-	-	-	-	-	-	-	-	-	0.7	0.7	0.7
	d_{-11}	-	-	-	-	-	-	-	-	3.1	2.2	2.2	2.2
	d_{-10}	-	-	-	-	-	-	-	5.5	4.6	3.7	3.7	3.7
	d_{-9}	-	-	-	-	-	-	7.9	7.0	6.1	5.2	5.2	5.2
	d_{-8}	-	-	-	-	-	10.0	9.1	8.5	7.6	6.7	6.7	6.7
	d_{-7}	-	-	-	-	12.4	11.5	10.6	10.0	9.1	8.5	8.5	8.5
	d_{-6}	-	-	-	14.8	13.9	13.0	12.4	11.8	10.9	10.3	10.3	10.3
	d_{-5}	-	-	17.2	16.3	15.4	14.5	13.9	13.3	12.4	12.1	12.1 / 6.1	12.1 / 6.1
	d_{-4}	-	-	19.0	17.8	16.9	16.3	15.4	15.1	14.2	13.9	13.9	13.9
	d_{-3}	-	20.8	20.5	19.3	18.4	17.8	17.2	16.9	16.3	15.7	15.7	15.7
	d_{-2}	-	22.6	22.0	21.1	20.2	19.6	19.3	19.0	18.4	17.8	17.8	17.8
	d_{-1}	-	24.4	23.8	22.6	22.0	21.7	21.4	21.1	20.5	19.6	19.6	19.6
	d_0	26.0	25.9	25.3	24.7	24.4	24.1	23.5	23.2	22.3	21.7	21.7	21.7 / 14.8
	d_1	-	27.7	27.1	26.8	26.8	26.2	25.6	25.0	24.4	24.1	24.1	24.1
	d_2	-	29.6	29.2	29.2	28.6	28.3	27.7	27.4	26.8	26.2	26.2	26.2
	d_3	-	31.7	31.7	31.1	30.8	30.5	30.2	29.6	28.9	28.0	28.0	28.0
	d_4	-	-	33.8	33.5	33.2	32.9	32.3	31.7	31.1	30.2	30.2	30.2
	d_5	-	-	36.5	35.9	35.6	35.0	34.4	34.1	33.5	32.6	32.6	32.6
	d_6	-	-	-	38.3	37.7	37.4	36.8	36.2	35.9	35.0	35.0	35.0
	d_7	-	-	-	-	40.1	39.5	39.2	38.6	38.3	37.4	37.4	37.4
	d_8	-	-	-	-	-	41.9	41.6	41.3	40.4	39.8	39.8	39.8
	d_9	-	-	-	-	-	-	44.3	43.7	43.1	42.2	42.2	42.2
	d_{10}	-	-	-	-	-	-	-	46.4	45.8	45.5	45.5	45.5
	d_{11}	-	-	-	-	-	-	-	-	48.5	47.9	47.9	47.9

The antenna scanning performance throughout the design process is shown in Figure 3a. The unifocal phase law achieves a high gain of 33.7 dBi at the focal panel position of d_0, but it rapidly drops as the panel shifts out of this position. Within the final panel translation range, which spans between d_{-12} and d_{11}, the unifocal phase law shows a minimum gain of 25.4 dBi, or approximately 8.3 dB of scan loss. After three iterations of the design process, the phase law has been optimized for the range between d_{-6} and d_6. This forces a drop to 32.5 dBi in maximum gain, but it also increases the minimum gain within this optimized range from 29.8 to 31.4 dBi (or from 25.4 to 27.0 dBi, considering the final panel translation range). After nine iterations, the phase law has been optimized for all panel positions from d_{-12} to d_{11}. This results in a new maximum gain of 31.4 dBi, and a minimum gain of 30.4 dBi. In other words, compared to the unifocal design, the minimum gain has been increased from 25.4 to 30.4 dBi, and scan loss has been reduced to only 1 dB.

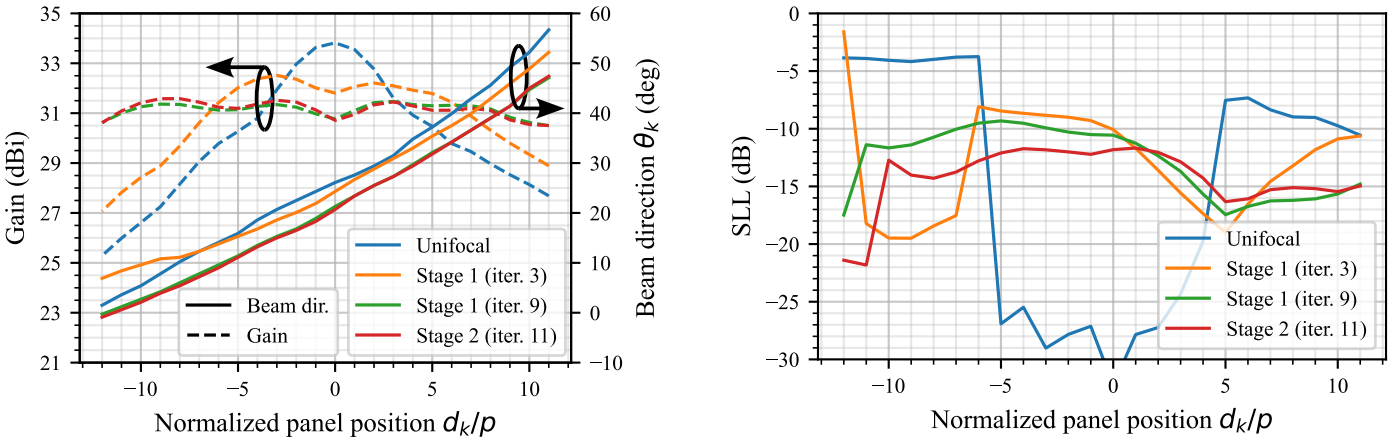

(**a**) (**b**)

Figure 3. Calculated scanning performance throughout the design process: main beam direction and gain (**a**) and SLL (**b**) for each panel position.

3.2. SLL Reduction

The design process above introduces unwanted phase aberrations on the reflected aperture field. These result in beam distortions in the form of high SLLs, which are particularly prominent at specific panel positions. As presented in Figure 3b, the maximum SLL after the scanning range optimization is −9.3 dB at d_{-5}. Ideally, these aberrations should be evenly spread across the entire scanning range so that no particular panel position is too affected. In order to mitigate the highest side lobes and to spread these aberrations more evenly across the scanning range, a second design stage is defined. The objective of this stage is to mitigate the SLLs of the most affected panel positions. The response of the RA panel will be refined to avoid partial collimation effects in the direction of the side lobes. To do so, an iterative approach similar to the first design stage will be used, except in this case the objective is to reduce collimation in the specific direction of the side lobes, as opposed to improving collimation in the direction of the main beam.

Each iteration begins by identifying the panel position with the highest side lobe, d_k. The side lobe direction, θ_k^{SL}, is selected as an additional intended beam direction for d_k. As a result, d_k has two radiation objectives as follows: one for collimating towards θ_k (fixed in the previous design stage) and the other for θ_k^{SL}. This secondary radiation direction is assigned a negative weight w_k^{SL} in the optimization process. Effectively, this means that when the optimization process will be biased to favor a phase law that collimates towards θ_k when the panel is at d_k (through a positive optimization weight w_k), while reducing

partial collimation effects towards the identified SLL direction θ_k^{SL} (through a negative weight w_k^{SL}).

This technique works by reducing collimation effects towards specific directions. For this reason, it can only be applied once the RA response is nearly finalized and the direction and level of the side lobes are well established. The response of the RA must not be altered significantly during this refinement stage; otherwise, it is possible for the side lobes to shift to a different direction rather than be suppressed. For this reason, this design stage is a refinement stage, where large changes to the phase law should be avoided. To that end, the set of panel positions and their radiation directions, as well as the optimization weight, are fixed after the ninth iteration (end of the first design stage). Furthermore, only two side-lobe suppression iterations are performed, and high values for $-w_k^{SL}$ are avoided. The two refined panel positions are d_{-5} and d_0, and the suppressed side-lobe angle is listed in Table 1. The effects of this refinement are shown in Figure 3, as follows: the main beam level and radiation directions are mostly unchanged between stages 1 and 2 (Figure 3a), but the maximum SLL is reduced from −9.3 dB to −11.7 dB (Figure 3b).

The initial and final phase responses and the offset between the two are shown in Figure 4. The −9 dB illumination taper is overlaid for the positions $d_{\pm 11}$ to highlight the region of the aperture that is most relevant for each panel position. The main differences between both responses occur on the edges of the panel. That is because the illumination is lower there for the central feed positions, and thus, more effective optimizations are possible with little effect on the other beams.

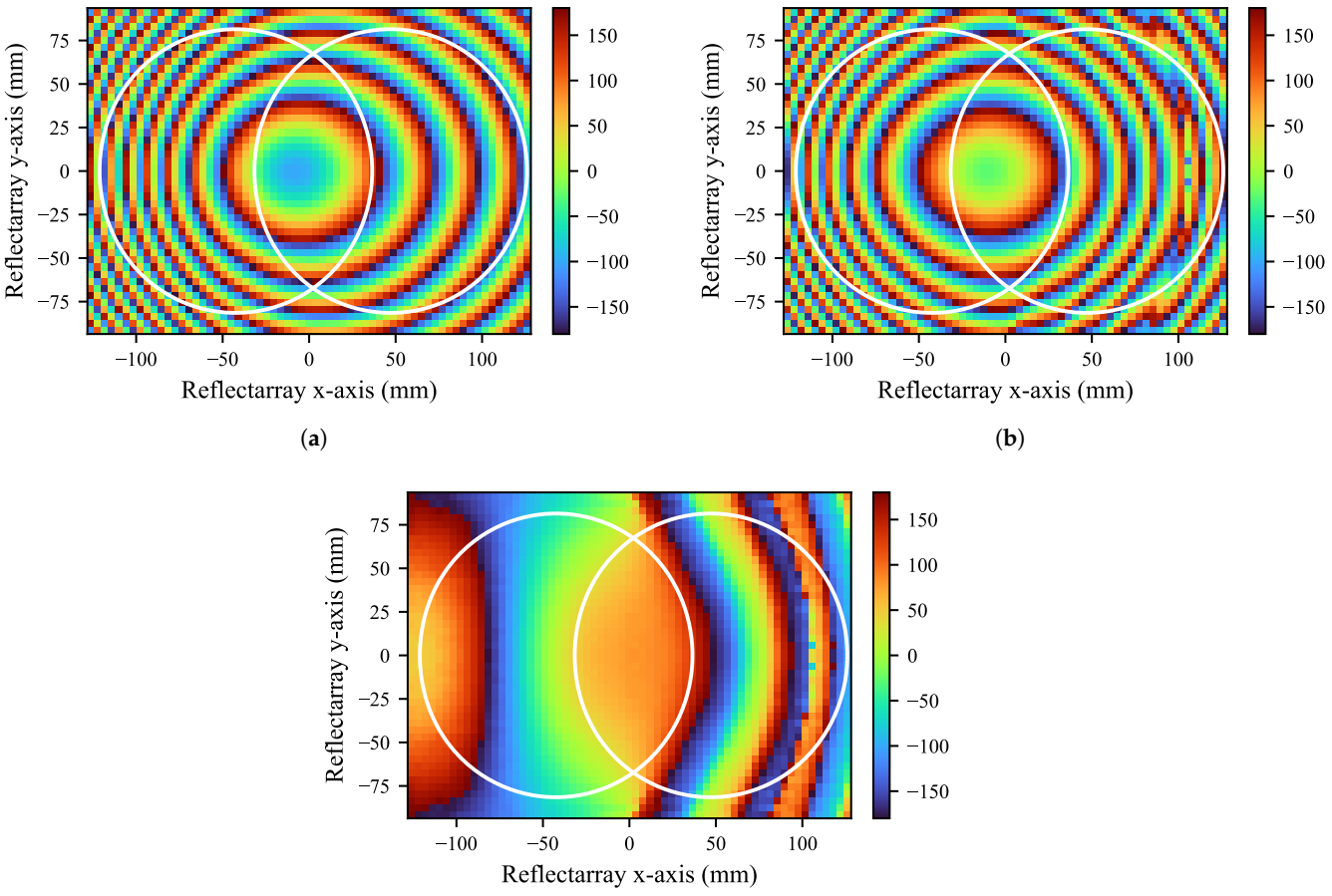

Figure 4. Calculated unifocal ($\phi_n^{(0)}$) (**a**) and optimized ($\phi_n^{(11)}$) (**b**) phase laws for the presented RA antenna. The difference between the two is shown in (**c**) in terms of $\phi_n^{(11)} - \phi_n^{(0)}$. The illumination taper contours at −9 dB for panel positions $d_{\pm 11}$ are overlaid in all three cases.

4. Experimental Validation

To validate the results from this work, a demonstrator is manufactured and measured. The optimized phase response from Figure 4b is implemented using the unit cell shown in Figure 5, consisting of three coplanar parallel dipoles of two different sizes. It is implemented on a thin, single-layer DiClad 880 substrate at 0.762 mm thickness, with a permittivity $\epsilon_r = 2.3$ and a loss tangent $\tan\delta = 0.005$. This cell has been introduced before in previous works [32,33]. The two dipole sizes resonate at two different frequencies, resulting in a smooth and highly linear phase response that can improve the bandwidth of the antenna. Its good angular stability is also particularly important for this phase-only design, as the angle from which each array element is excited depends on the position of the panel, and a stable cell response is desired. With the dimensions listed in Figure 5a, a full phase cycle (360 degrees) is covered while losses are kept below 0.5 dB.

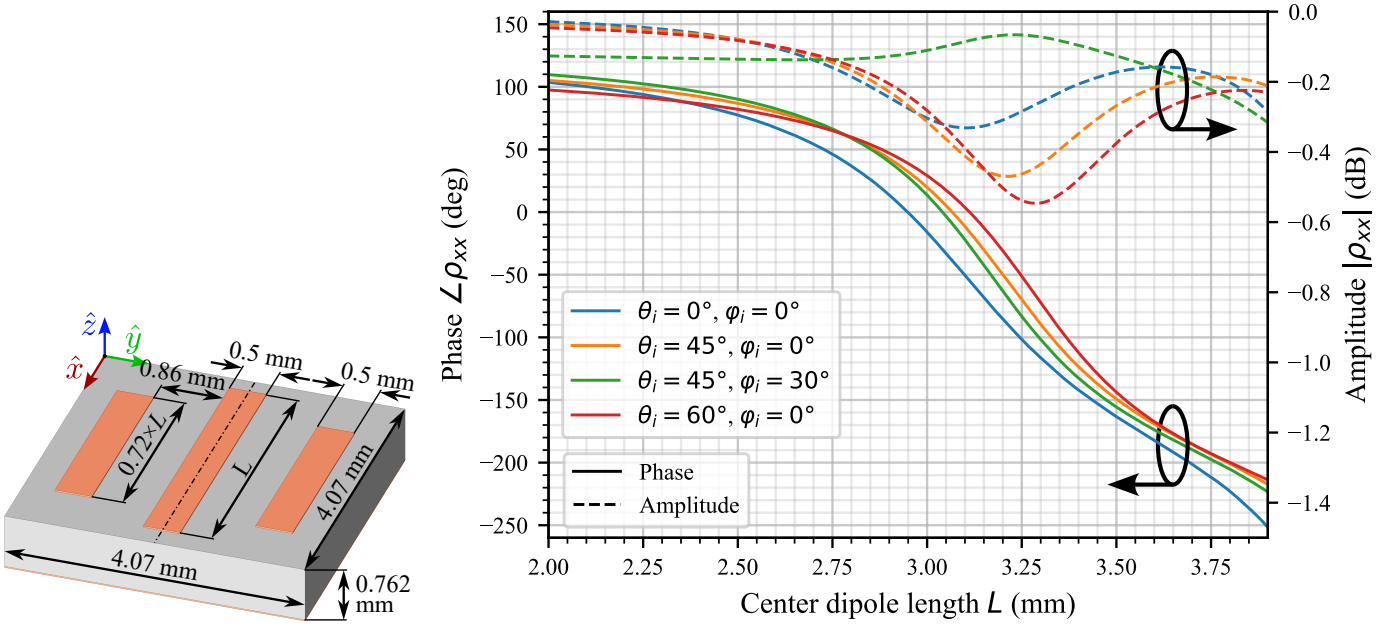

(**a**) (**b**)

Figure 5. Reflectarray unit cell geometry (**a**) and its direct reflection coefficient ρ_{xx} at 29.5 GHz (**b**), simulated in Ansys HFSS under periodic boundary conditions.

The manufactured demonstrator is shown in Figure 6. The panel slides along a 3D-printed rail, and it is fixed at multiple predefined positions for the measurements. The full 3D antenna gain pattern is measured at these positions. Figure 7 compares the gain cuts along the scanned plane between the measurements and the calculated predictions at the design frequency of 29.5 GHz. A good match is observed, with the prototype achieving a maximum gain of 31.6 dBi with a scan loss of 1.1 dB for over 45 degrees of scanning range. Scanning outside the optimization range at d_{12} results in a 50-degree beam tilt with losses of 2.8 dB. Side lobes are kept below −9.9 dB. Since the support structure is mostly 3D-printed and it contains moving parts, any discrepancies in the results may be attributed to minor alignment errors. The aperture efficiency at 29.5 GHz is 24.7%, which is calculated by comparing the antenna gain with that of an ideal, uniformly illuminated aperture of the same size [31]. This antenna design, however, is based on a partial aperture overlap among panel positions, meaning that only part of the RA aperture has a noticeable contribution to the radiated field at any given panel position. If we only consider the aperture area where the illumination taper is over −12 dB, the aperture efficiency is increased to 34.6%.

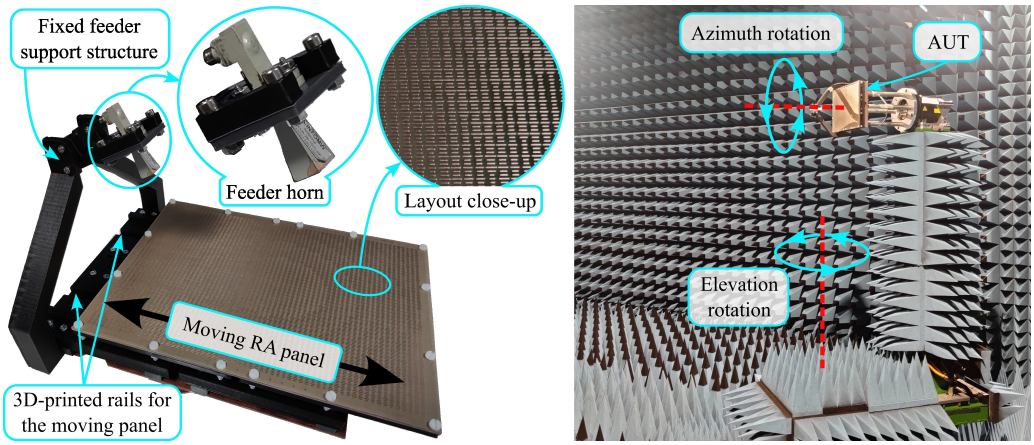

Figure 6. Manufactured demonstrator with a sliding rail (**left**) in our spherical range measurement facility (**right**).

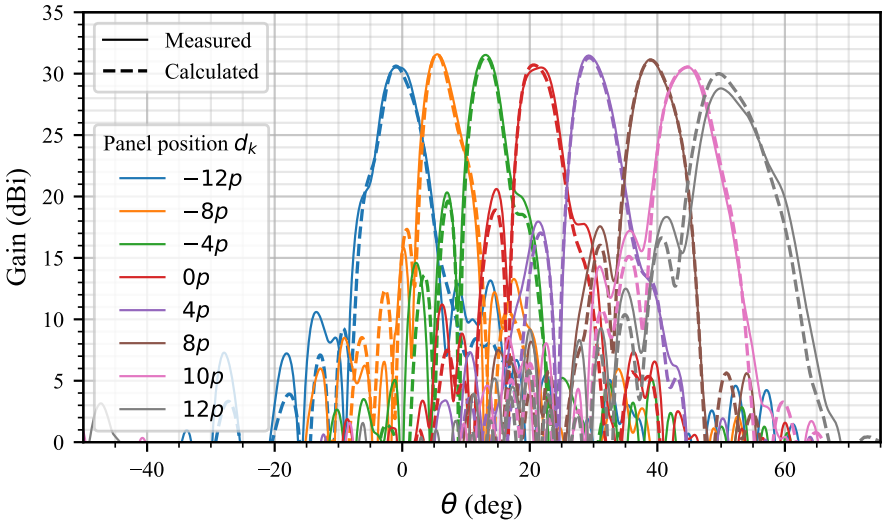

Figure 7. Measured and calculated gain cuts at $\varphi = 0°$ and 29.5 GHz, for different predefined panel positions, where $p = 4.07$ mm. For the calculation, the response of every cell in the array was simulated in HFSS.

The measured in-band antenna performance is presented in Figure 8. The scanning range is most affected at highly obliquely radiating positions, and particularly below the design frequency. For a 45-degree scanning range, scan losses are kept below 2 dB, from 28.5 to over 32 GHz, and below 3 dB, starting at 28 GHz. To compare these measurements with the expected performance, the feeding horn and the RA layout are also simulated over a broad band, and the radiation pattern is calculated at multiple panel positions. Focusing exclusively on the set of measured positions that fall within the optimized translation range, the minimum and maximum beam levels among these positions are represented in Figure 9 for both measurements and simulations. The measured results show a good match with the simulations, and the variation in maximum gain of the measured prototype is only 0.83 dB between 28.5 GHz and 32.0 GHz (11.9% bandwidth).

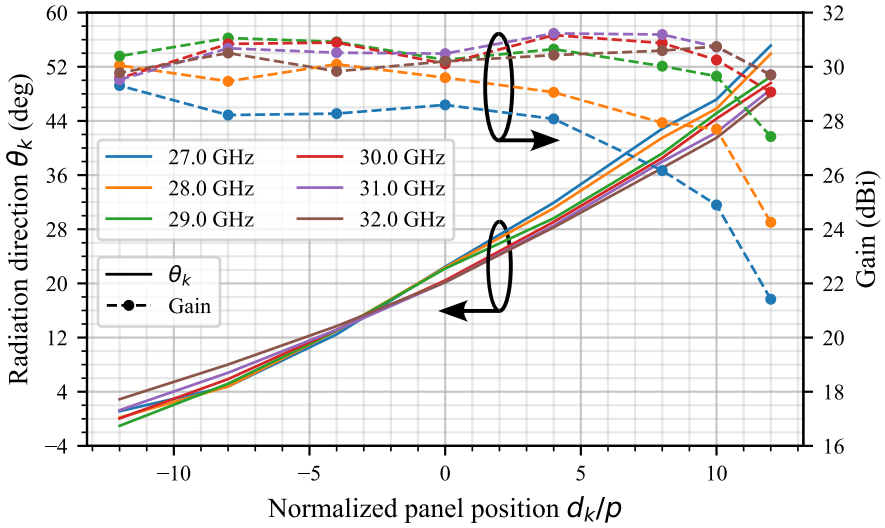

Figure 8. Measured in-band scanning performance.

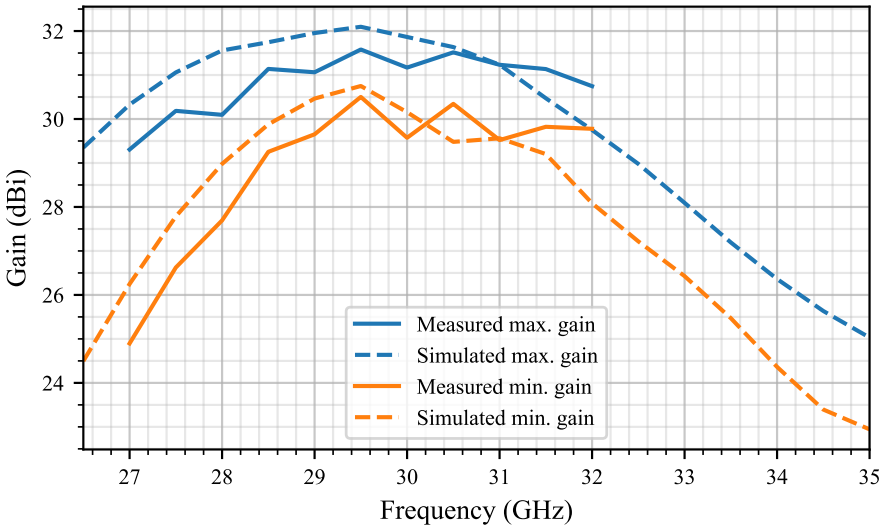

Figure 9. Broadband demonstrator performance in terms of the maximum and minimum beam levels within the optimized panel translation range.

Compared to other beam-scanning reflectarray designs (see Table 2), the proposed antenna prioritizes mechanical simplicity by relying on a single stepper motor to achieve linear in-plane panel translations. This contrasts with more complex mechanical implementations, such as systems employing multiple moving components like [22] or feed translations like [23]. These more complex systems benefit from a more flexible antenna geometry that enhances their scanning performance at the expense of added complexity. Some of the listed designs like [17,19] overcome their mechanical complexity by targeting fixed multi-beam configurations using multiple coexisting feeds, as opposed to having a single feed capable of facilitating the smooth, continuous steering of the beam. Compared to the entries listed, the presented design achieves the highest gain (31.6 dBi) while maintaining the smallest focal ratio ($F/D = 0.47$) and very low scanning losses. A particularly relevant entry is [27], which uses a similar scanning mechanism using a rollable panel instead of a moving one. Compared to [27], our design achieves a significantly higher maximum gain (exceeding it by more than 6 dB), a lower scan loss over the same scanning range, and improved aperture efficiency, all while using a more compact and structurally efficient configuration. However, because of this compact structure, side lobes are increased even after the SLL mitigation stage used during the design process.

Table 2. Comparison with other related beam scanning designs.

Ref.	Approach	CS/MB [1]	Freq. (GHz)	Max. Gain (dBi)	Scan Range (deg)	Scan Loss (dB)	Apert. Effic. [2]	*F*/*D*	Band-Width	SLL (dB)
[19]	Folded RA with polarizer, feeders embedded in panel	MB	26.5	24.6	58	2.1	15.0%	0.71	12.6% @ 3 dB	−8.5
[22]	Folded RA, Risley prism using two rotating panels	CS	10.0	21.5	$\theta \leq 45$ (2D)	2.3	31.2%	0.84	11.5% @ 3 dB	NA [1]
[17]	Multiple feeds along tilted focal arc	MB	29.5	28.2	90	0.5	6.8%	0.58	6.8% @ 1 dB	NA [1]
[23]	Feed movements along focal arc and panel rotations	CS	12.0	26.2	140	4.9	42.5%	1.0	4.2% @ 1 dB	NA [1]
[27]	Linear panel translations using rollable panel	CS	14.0	25.1	42	1.5	17.9%	0.8	NA [1]	−15.0
This work	In-plane linear panel translations	CS	29.5	31.6	45	1.1	24.7%	0.47	11.9% @ 1 dB	−9.9

[1] CS: Continuous Scanning; MB: Multi-beam; NA: Not Available. [2] Efficiency is calculated for all entries using the definition stated in this paper. Other equally valid criteria may be used in the listed works.

5. Conclusions

A 1D beam-scanning RA antenna is presented as a cost-effective solution for millimeter-wave satellite communication terminals. The antenna is designed to prioritize mechanical simplicity while featuring a remarkably low focal ratio of $F/D_y = 0.47$. Despite using a simple steering approach based on in-plane panel movements, a continuous scanning range of 45 degrees is covered with a low scan loss of only 1.1 dB and a gain of 31.6 dBi. Compared to existing works, this antenna achieves a higher gain and comparable or lower scanning losses while featuring a significantly more compact form factor. To design this antenna, a multi-stage process is used. First, the scanning range is gradually expanded, while ensuring a highly uniform beam level across the entire scanning range. Once the desired range is achieved, a novel technique is proposed to reduce the SLLs without degrading the antenna's performance. To do so, a multi-focal optimization is re-purposed to negatively bias collimation in the direction of the side-lobe, achieving a SLL reduction of up to 2.3 dB. To the best of the authors' knowledge, this is the first application of a multi-focal optimization in such a way. Its use was motivated by the particular challenges created by such a low focal ratio, but this technique should be applicable to other future mechanically scanned reflectarray antenna designs.

Author Contributions: Conceptualization, A.G.-Á., S.A.M. and C.A.F.; investigation, A.G.-Á., S.A.M., M.A., M.R.P. and C.A.F.; design process implementation, A.G.-Á.; validation (simulation), S.A.M. and C.A.F.; validation (measurements), A.G.-Á., M.A. and M.R.P.; writing—original draft preparation, A.G.-Á.; writing—review and editing, A.G.-Á., S.A.M., M.A., M.R.P. and C.A.F.; supervision, M.A. and M.R.P. All authors have read and agreed to the published version of the manuscript.

Funding: This work was supported in part by MCIN/AEI/10.13039/501100011033 under grants PID2020-114172RB-C21, PID2023-146246OB-C32, and TED2021-130650B-C22, co-funded by the EU (European Union) "NextGenerationEU"/PRTR; by Ministerio de Educación y Formación Profesional, under grant FPU20/07267; and by FCT/MECI through national funds and, when applicable, co-funded EU funds under UID/50008: Instituto de Telecomunicaçoes.

Institutional Review Board Statement: Not applicable.

Informed Consent Statement: Not applicable.

Data Availability Statement: The raw data supporting the conclusions of this article will be made available by the authors upon request.

Conflicts of Interest: The authors declare no conflicts of interest.

References

1. del Portillo, I.; Cameron, B.G.; Crawley, E.F. A technical comparison of three low earth orbit satellite constellation systems to provide global broadband. *Acta Astronaut.* **2019**, *159*, 123–135. [CrossRef]
2. Merino-Fernandez, I.; Khemchandani, S.L.; del Pino, J.; Saiz-Perez, J. Phased Array Antenna Analysis Workflow Applied to Gateways for LEO Satellite Communications. *Sensors* **2022**, *22*, 9406. [CrossRef] [PubMed]
3. Correia, R.; Varum, T.; Matos, J.N.; Oliveira, A.; Carvalho, N.B. User Terminal Segments for Low-Earth Orbit Satellite Constellations: Commercial Systems and Innovative Research Ideas. *IEEE Microw. Mag.* **2022**, *23*, 47–58. [CrossRef]
4. Encinar, J. Design of two-layer printed reflectarrays using patches of variable size. *IEEE Trans. Antennas Propag.* **2001**, *49*, 1403–1410. [CrossRef]
5. Florencio, R.; Encinar, J.A.; Boix, R.R.; Losada, V.; Toso, G. Reflectarray Antennas for Dual Polarization and Broadband Telecom Satellite Applications. *IEEE Trans. Antennas Propag.* **2015**, *63*, 1234–1246. [CrossRef]
6. Wu, G.B.; Qu, S.W.; Yang, S.; Chan, C.H. Broadband, Single-Layer Dual Circularly Polarized Reflectarrays with Linearly Polarized Feed. *IEEE Trans. Antennas Propag.* **2016**, *64*, 4235–4241. [CrossRef]
7. Nayeri, P.; Liang, M.; Sabory-García, R.A.; Tuo, M.; Yang, F.; Gehm, M.; Xin, H.; Elsherbeni, A.Z. 3D Printed Dielectric Reflectarrays: Low-Cost High-Gain Antennas at Sub-Millimeter Waves. *IEEE Trans. Antennas Propag.* **2014**, *62*, 2000–2008. [CrossRef]
8. Zhu, J.; Yang, Y.; Mcgloin, D.; Liao, S.; Xue, Q. 3-D Printed All-Dielectric Dual-Band Broadband Reflectarray with a Large Frequency Ratio. *IEEE Trans. Antennas Propag.* **2021**, *69*, 7035–7040. [CrossRef]
9. Vaquero, Á.F.; Teixeira, J.; Matos, S.A.; Arrebola, M.; Costa, J.R.; Felício, J.M.; Fernandes, C.A.; Fonseca, N.J.G. Design of Low-Profile Transmitarray Antennas with Wide Mechanical Beam Steering at Millimeter Waves. *IEEE Trans. Antennas Propag.* **2023**, *71*, 3713–3718. [CrossRef]
10. Samaiyar, A.; Abdelrahman, A.H.; Boskovic, L.B.; Filipovic, D.S. Extreme Offset-Fed Reflectarray Antenna for Compact Deployable Platforms. *IEEE Antennas Wirel. Propag. Lett.* **2019**, *18*, 1139–1143. [CrossRef]
11. Imaz-Lueje, B.; Pino, M.R.; Arrebola, M. Deployable Multi-Faceted Reflectarray Antenna in Offset Configuration with Band Enhancement. *IEEE Trans. Antennas Propag.* **2022**, *70*, 11686–11696. [CrossRef]
12. Trampler, M.E.; Lovato, R.E.; Gong, X. Dual-Resonance Continuously Beam-Scanning X-Band Reflectarray Antenna. *IEEE Trans. Antennas Propag.* **2020**, *68*, 6080–6087. [CrossRef]
13. Kamoda, H.; Iwasaki, T.; Tsumochi, J.; Kuki, T.; Hashimoto, O. 60-GHz Electronically Reconfigurable Large Reflectarray Using Single-Bit Phase Shifters. *IEEE Trans. Antennas Propag.* **2011**, *59*, 2524–2531. [CrossRef]
14. Clemente, A.; Diaby, F.; Palma, L.D.; Dussopt, L.; Sauleau, R. Experimental Validation of a 2-Bit Reconfigurable Unit-Cell for Transmitarrays at Ka-Band. *IEEE Access* **2020**, *8*, 114991–114997. [CrossRef]
15. Debogovic, T.; Perruisseau-Carrier, J. Low Loss MEMS-Reconfigurable 1-Bit Reflectarray Cell with Dual-Linear Polarization. *IEEE Trans. Antennas Propag.* **2014**, *62*, 5055–5060. [CrossRef]
16. Cheng, C.C.; Abbaspour-Tamijani, A.; Lakshminarayanan, B. Reconfigurable Lens-Array with Monolithically Integrated MEMS Switches. In Proceedings of the 2008 38th European Microwave Conference, Amsterdam, The Netherlands, 27–31 October 2008; pp. 112–115. [CrossRef]
17. Gómez-Álvarez, A.; Vaquero, Á.F.; Arrebola, M.; Pino, M.R. Multibeam Compact Reflectarray Antenna with Low Scan Loss and Wide-Angle Performance Using a Multi-Feed Configuration. *IEEE Open J. Antennas Propag.* **2024**, *5*, 1095–1107. [CrossRef]
18. Hu, Y.; Hong, W.; Jiang, Z.H. A Multibeam Folded Reflectarray Antenna with Wide Coverage and Integrated Primary Sources for Millimeter-Wave Massive MIMO Applications. *IEEE Trans. Antennas Propag.* **2018**, *66*, 6875–6882. [CrossRef]
19. Yu, Z.Y.; Zhang, Y.H.; He, S.Y.; Gao, H.T.; Chen, H.T.; Zhu, G.Q. A Wide-Angle Coverage and Low Scan Loss Beam Steering Circularly Polarized Folded Reflectarray Antenna for Millimeter-Wave Applications. *IEEE Trans. Antennas Propag.* **2022**, *70*, 2656–2667. [CrossRef]
20. Matos, S.A.; Fonseca, N.J.G.; Serra, J.C.; Felício, J.M.; Costa, J.R.; Fernandes, C.A. Generalized Risley Prism for Beam-Steering Transmit Arrays with Reduced Grating Lobes. *IEEE Trans. Antennas Propag.* **2023**, *71*, 8420–8428. [CrossRef]
21. Lei, H.; Zhong, Y.C.; Jia, Y.; Zhu, J.; Liu, Z.X.; Chen, Y.N.; Liu, Y. A Low-Profile Risley-Prism-Based 2-D Beam-Scanning Circularly Polarized Folded Transmitarray Antenna at Ku-Band. *IEEE Trans. Antennas Propag.* **2023**, *71*, 6173–6178. [CrossRef]
22. Han, Z.; Du, Y.; Li, X.; Li, J. A 2-D Beam-Scanning Circularly Polarized Folded Reflectarray Antenna Based on Risley Prism at X-Band. *IEEE Trans. Antennas Propag.* **2024**, *72*, 6765–6770. [CrossRef]
23. Wu, G.B.; Qu, S.W.; Yang, S. Wide-Angle Beam-Scanning Reflectarray with Mechanical Steering. *IEEE Trans. Antennas Propag.* **2018**, *66*, 172–181. [CrossRef]
24. Wu, G.B.; Qu, S.W.; Yang, S.; Chan, C.H. Low-Cost 1-D Beam-Steering Reflectarray with ±70° Scan Coverage. *IEEE Trans. Antennas Propag.* **2020**, *68*, 5009–5014. [CrossRef]

25. Nayeri, P.; Yang, F.; Elsherbeni, A.Z. Bifocal Design and Aperture Phase Optimizations of Reflectarray Antennas for Wide-Angle Beam Scanning Performance. *IEEE Trans. Antennas Propag.* **2013**, *61*, 4588–4597. [CrossRef]
26. Cui, Y.; Bahr, R.; Nauroze, S.A.; Cheng, T.; Almoneef, T.S.; Tentzeris, M.M. 3D Printed "Kirigami"-Inspired Deployable Bi-Focal Beam-Scanning Dielectric Reflectarray Antenna for mm-Wave Applications. *IEEE Trans. Antennas Propag.* **2022**, *70*, 7683–7690. [CrossRef]
27. Rubio, A.J.; Kaddour, A.S.; Georgakopoulos, S.V. A Mechanically Rollable Reflectarray with Beam-Scanning Capabilities. *IEEE Open J. Antennas Propag.* **2022**, *3*, 1180–1190. [CrossRef]
28. *Ansys® HFSS*, Release 2023R1; Ansys, Inc.: Canonsburg, PA, USA, 2023.
29. Huang, J.; Encinar, J.A. *Reflectarray Antennas*; IEEE Press Series on Electromagnetic Wave Theory; Wiley: Hoboken, NJ, USA, 2007.
30. Lo, Y.T. Array theory. In *Antenna Handbook: Theory, Applications, and Design*; Lo, Y.T., Lee, S.W., Eds.; Springer: Boston, MA, USA, 1988; pp. 713–803. [CrossRef]
31. Stutzman, W.; Thiele, G. *Antenna Theory and Design*, 3rd ed.; Antenna Theory and Design; Wiley: Hoboken, NJ, USA, 2013.
32. Carrasco, E.; Barba, M.; Encinar, J.A.; Arrebola, M.; Rossi, F.; Freni, A. Design, Manufacture and Test of a Low-Cost Shaped-Beam Reflectarray Using a Single Layer of Varying-Sized Printed Dipoles. *IEEE Trans. Antennas Propag.* **2013**, *61*, 3077–3085. [CrossRef]
33. Florencio, R.; Boix, R.R.; Carrasco, E.; Encinar, J.A.; Losada, V. Efficient numerical tool for the analysis and design of reflectarrays based on cells with three parallel dipoles. *Microw. Opt. Technol. Lett.* **2013**, *55*, 1212–1216. [CrossRef]